Supporting Information

A cilia-inspired micropatterned sensor with a high-permittivity dielectric hydrogel for ultrasensitive mechanoreception both in air and underwater

Yuanyuan Wang, Jiaqi Liao, Chencong Liu, Qingfeng Sun*, Julia L. Shamshina*, Xiaoping Shen*

Y. Wang, J. Liao, C. Liu, Q. Sun, X. Shen

College of Chemistry and Materials Engineering

Zhejiang A&F University

Hangzhou 311300, China

J. L. Shamshina

Fiber and Biopolymer Research Institute

Department of Plant and Soil Science

Texas Tech University

Lubbock, TX 79409, USA

E-mail: qfsun@zafu.edu.cn; jshamshi@ttu.edu, xpshen@zafu.edu.cn

Content:

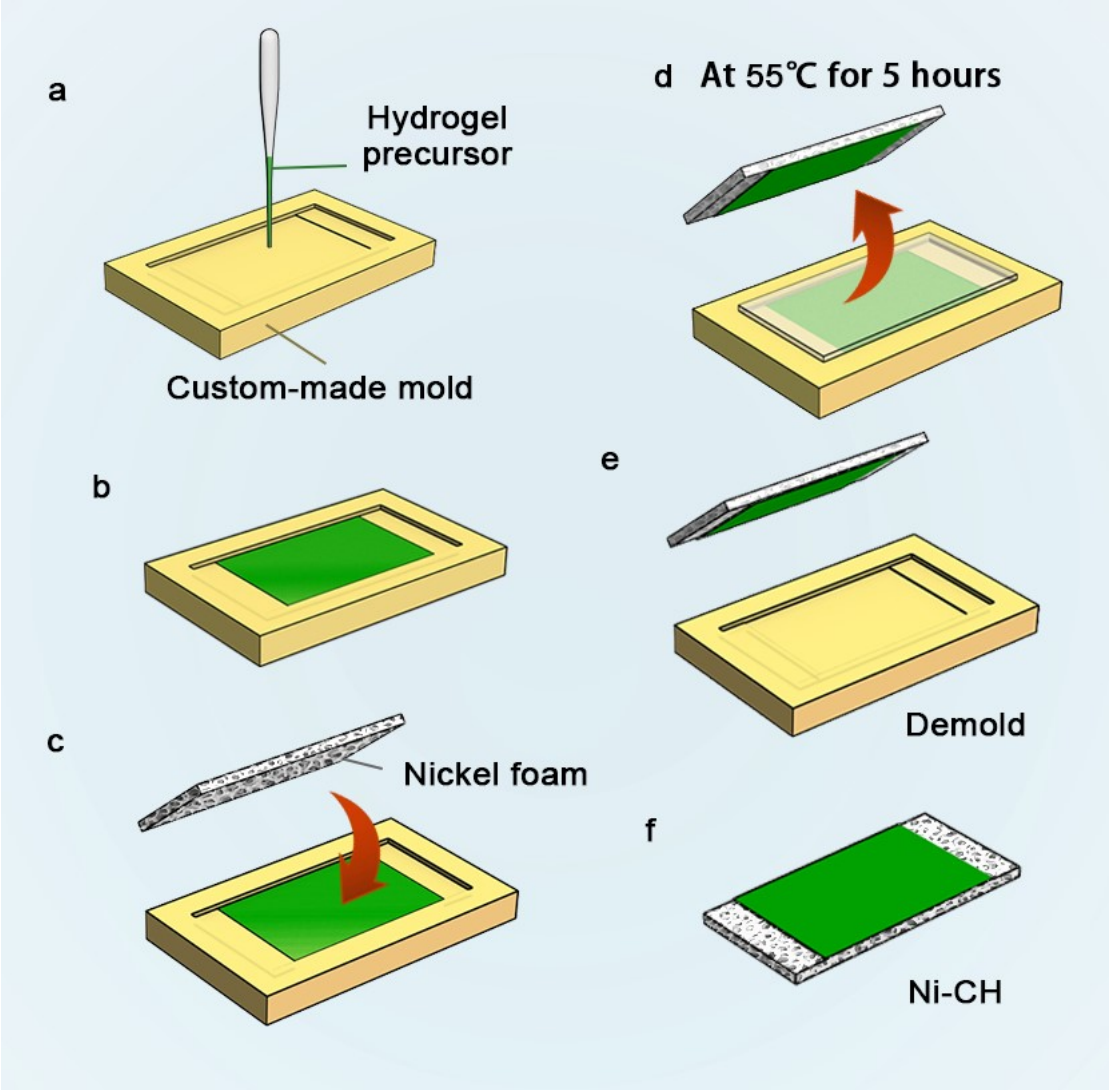

Fig. S1. Preparation of Ni-CH on a nickel foam using a custom-made mold.

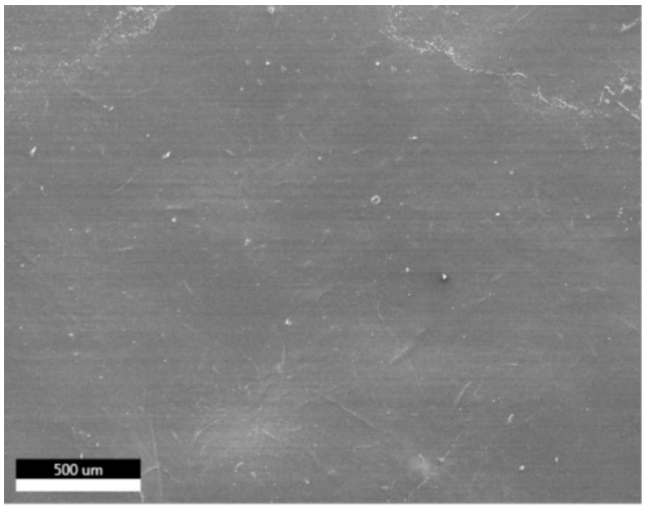

Fig. S2. SEM image of the surface of Ni-CH.

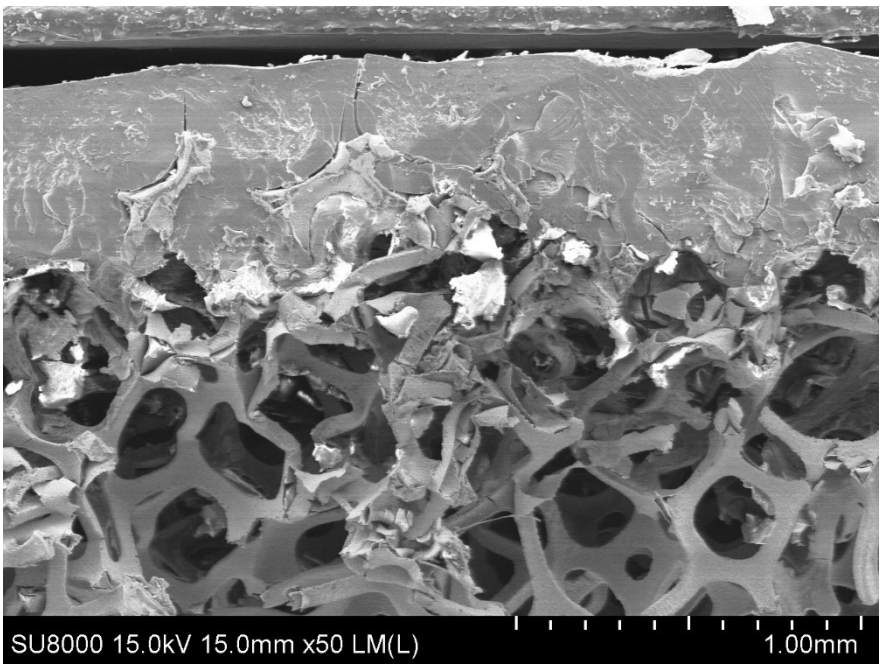

Fig. S3. SEM image captured from a lateral perspective of the Ni-CH on a nickel foam.

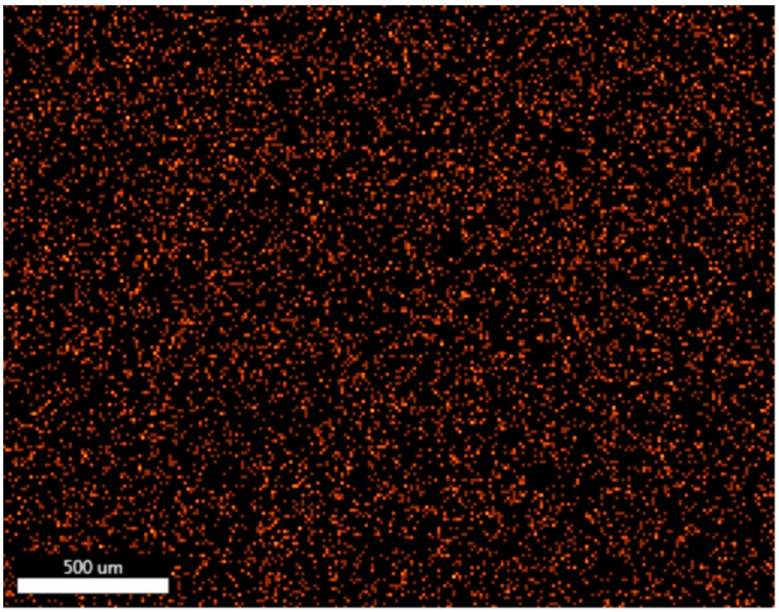

Fig. S4. Ni elemental mapping on the surface of Ni-CH.

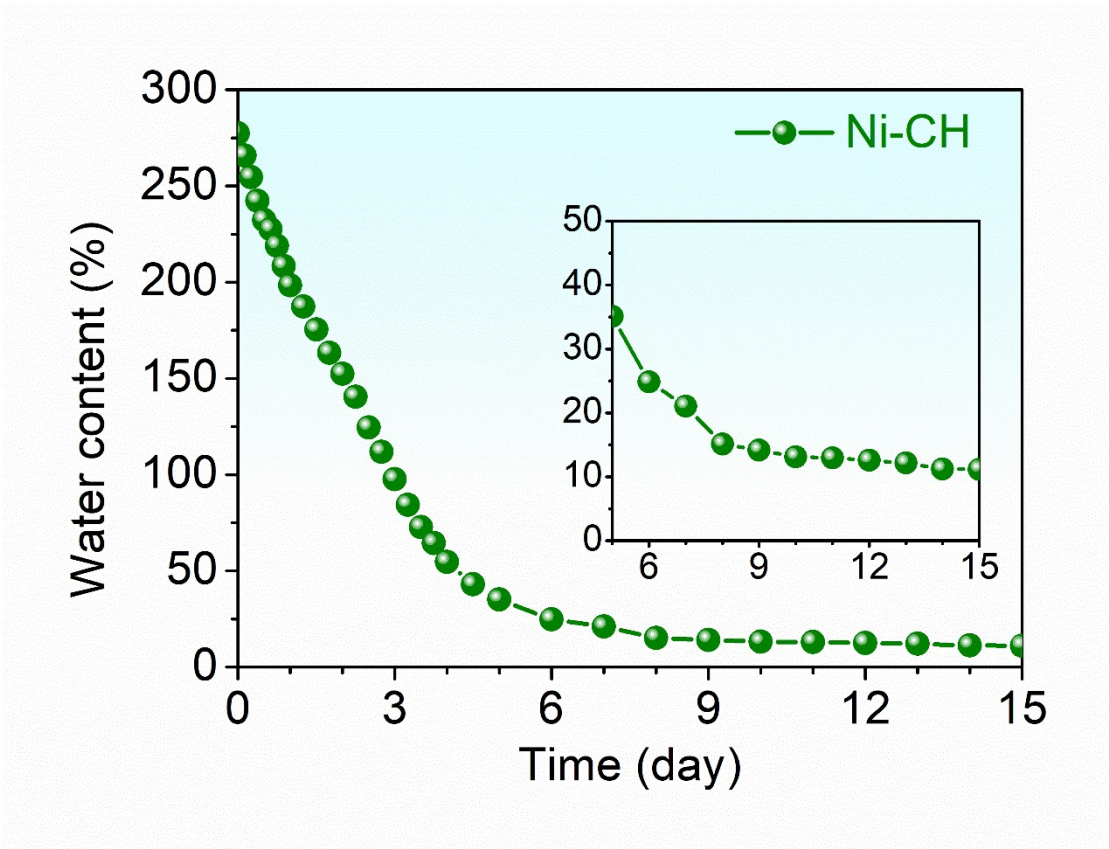

Fig. S5. Water content of Ni-CH measured at room temperature (ranging within 25-30 °C) and room humidity (ranging within 40-80%).

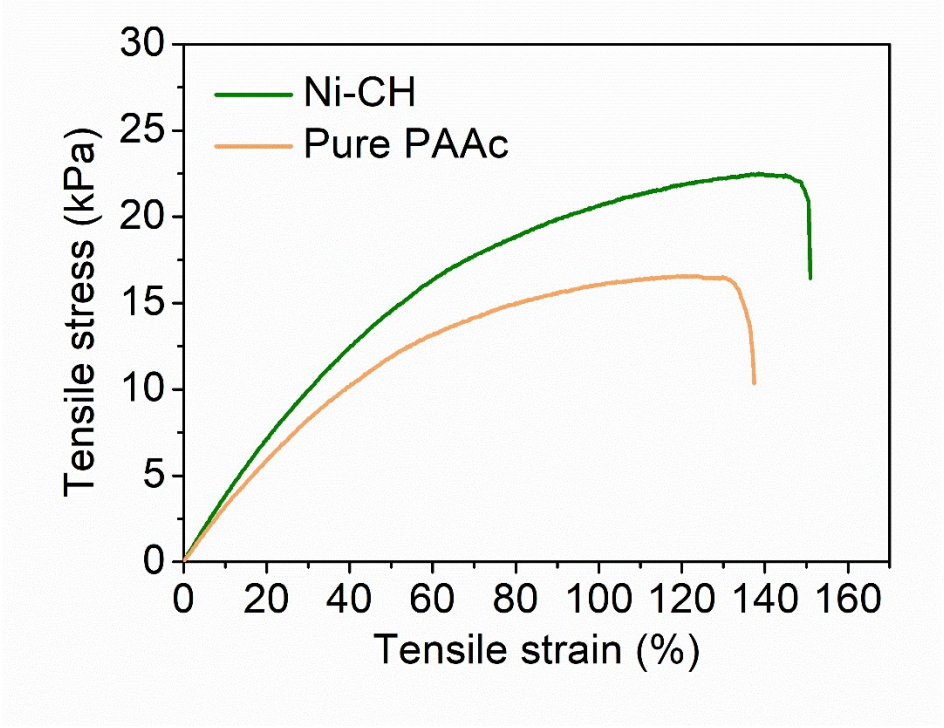

Fig. S6. Tensile stress-strain curves of Ni-CH and pure PAAc hydrogels.

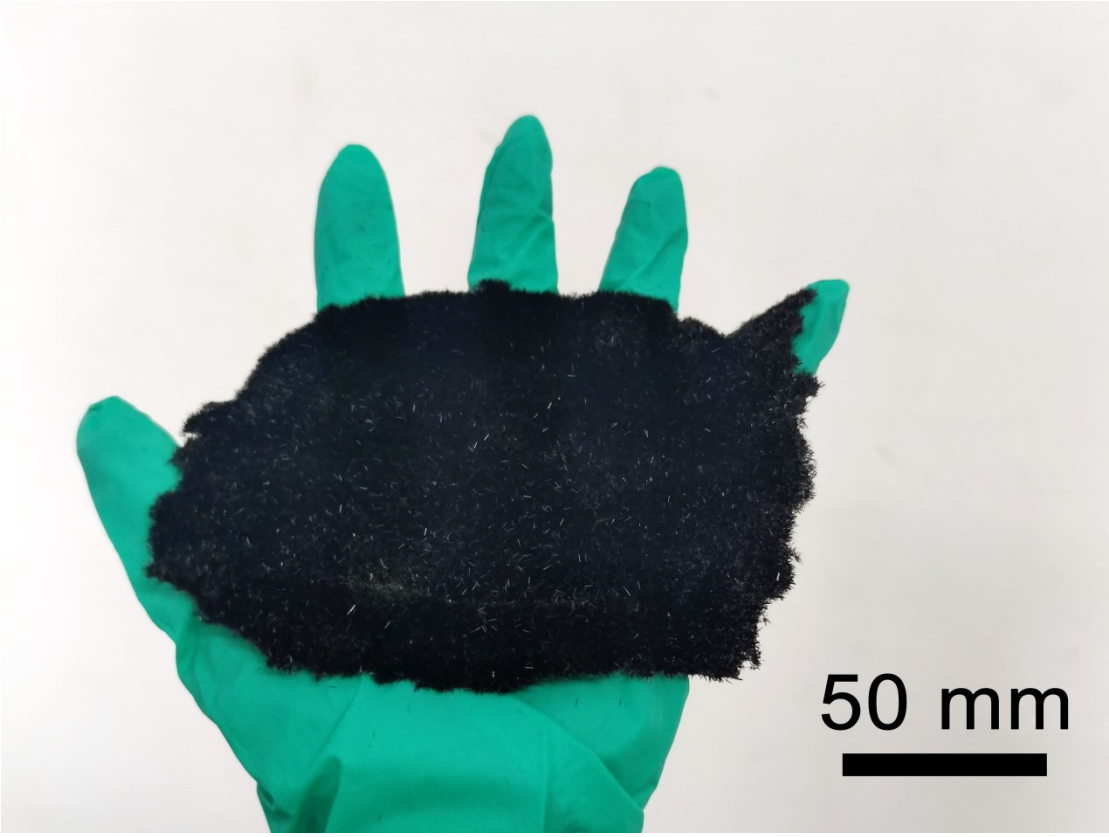

Fig. S7. Picture of the large-area hybrid conductive membrane.

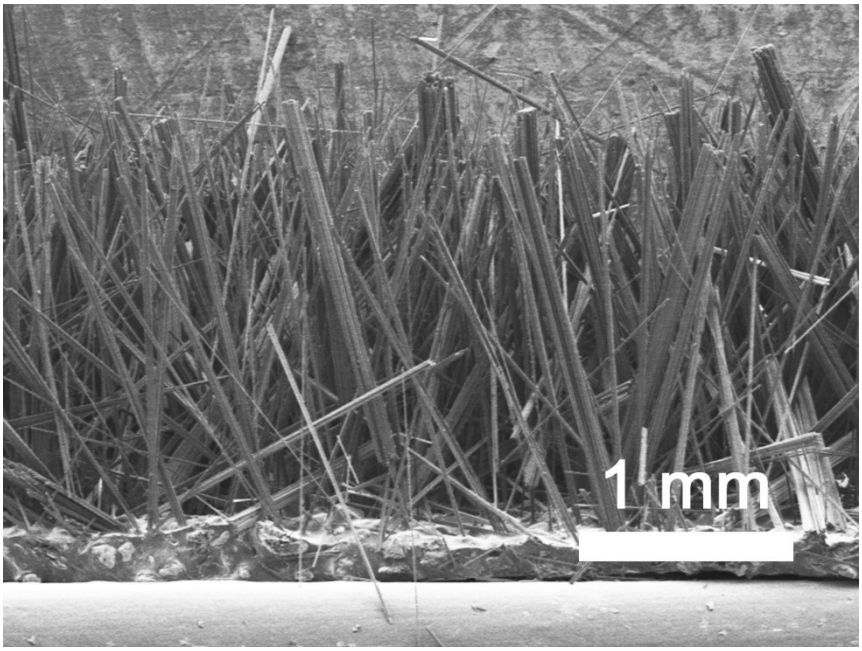

Fig. S8. SEM image of the CF electrode after cycling tests.

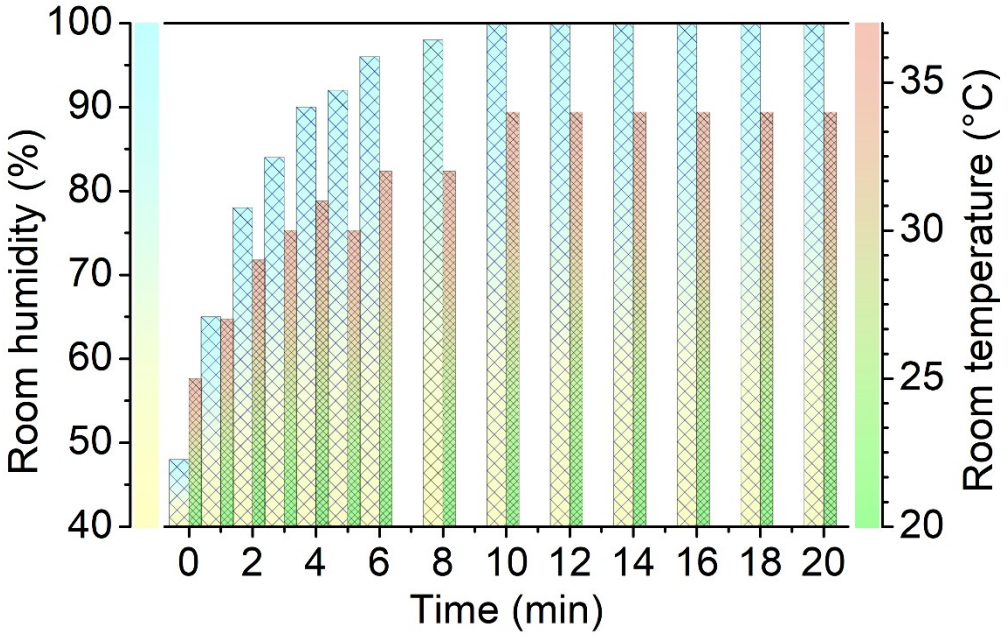

Fig. S9. Temperature and humidity recording inside a mask during respiration monitoring.

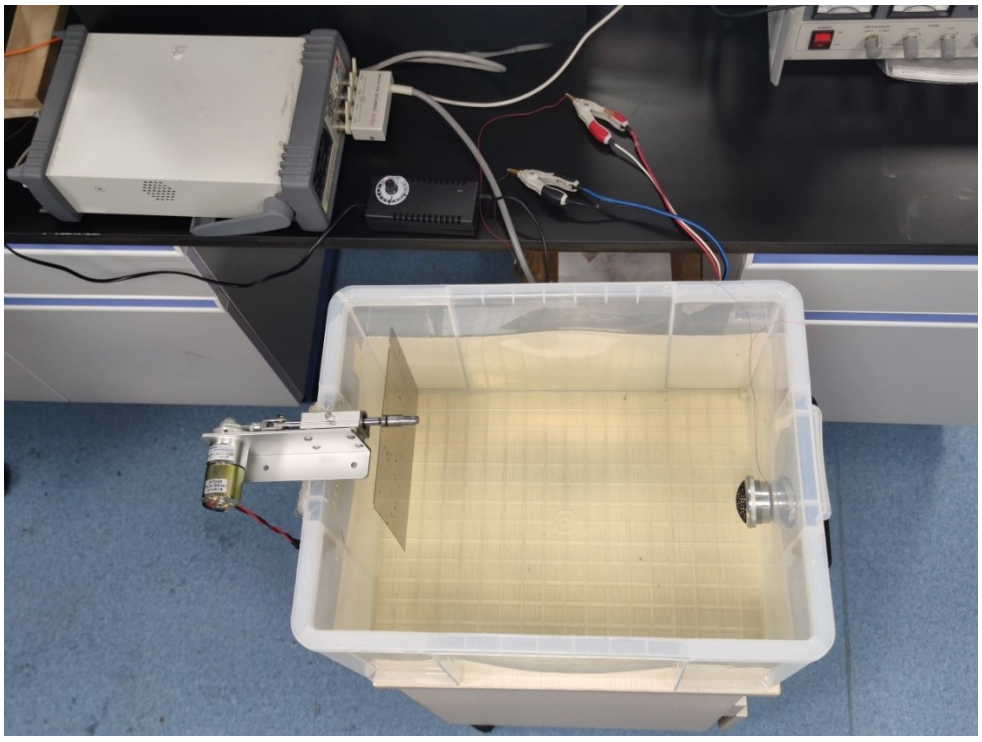

Fig. S10. The custom water wave generation system.

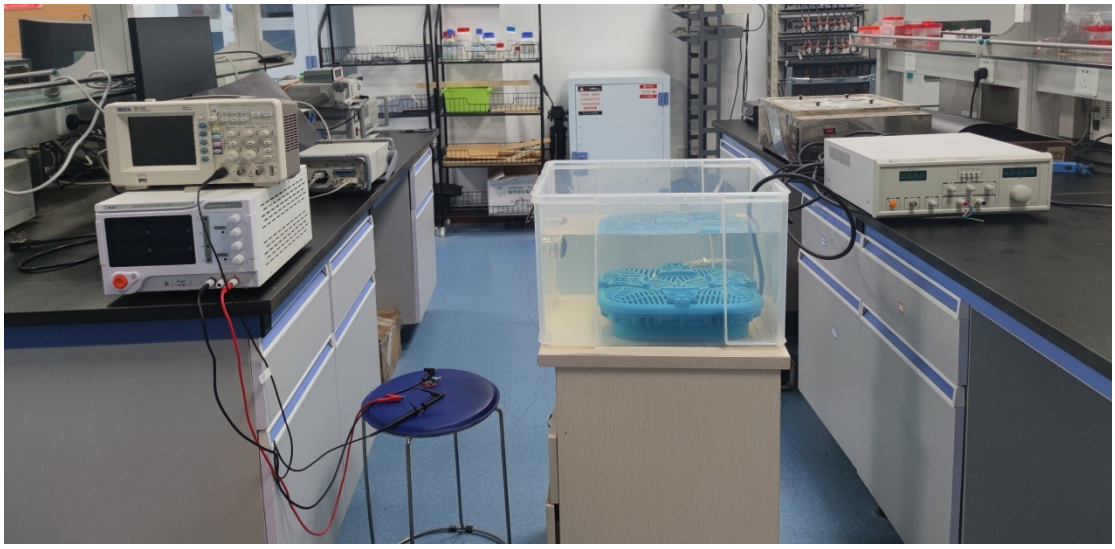

Fig. S11. The test setup of a hydrophone.

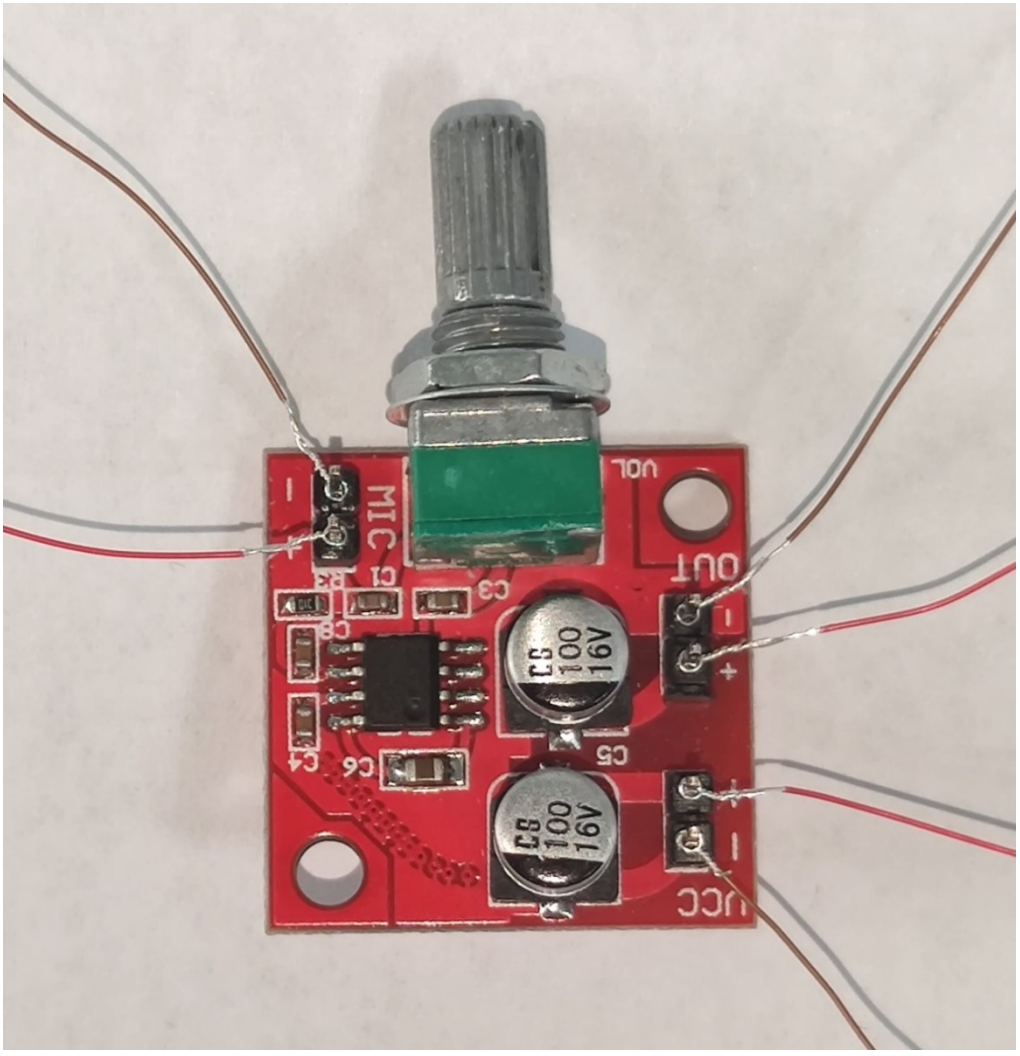

Fig. S12. Circuit for the signal transformation from capacitance to voltage. MIC for the capacitance input, UCC for the power supply (4.5 V), OUT for voltage output.

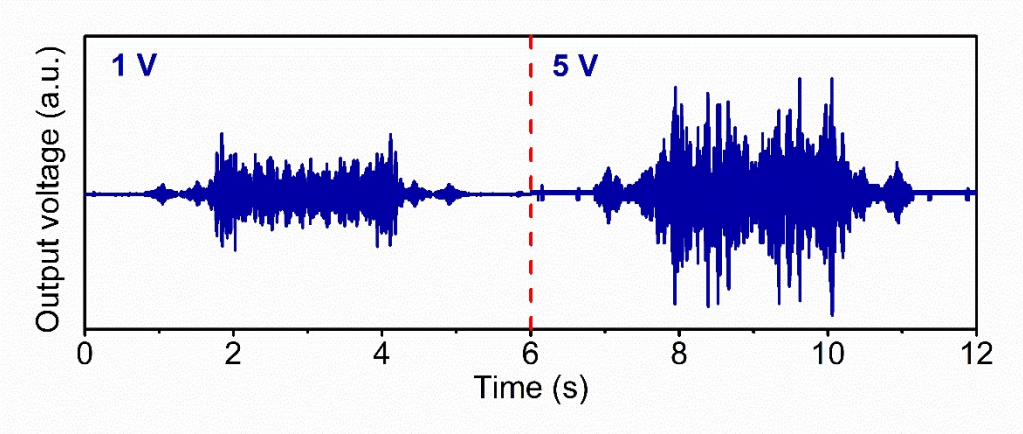

Fig. S13. Dependence of acoustic wave detection voltage of the cilia-inspired sensor on the acoustic wave intensity with a sweep frequency method (20-20k Hz).

Calculation of sound sensitivity (S)

If the voltage signal of hydrophone is $10^{-3.5}$V under a sound pressure of 1Pa, then the sensitivity is:

$10^{-3.5}$ V / 1 Pa = $10^{-3.5}$V/Pa.

The S can be further defined as:

$\boldsymbol{S}$= 20×lg[($10^{-3.5}$V/Pa) / (1 V/μPa)] = 20×lg($10^{-9.5}$) = -190 dB

Calculation of sound pressure

Firstly, the environmental noise is determined when no extra sound generator was used. After FFT analyses of the voltage output, the voltage spectra for the surrounding noise is pbtained. If the voltage at 2 kHz is 2×10^{-2} V, then the surrounding noise at 2 kHz is 20×lg(20^{-2})=-34 dB.

If the S value of the hydrophone is -192 dB, then the sound pressure level (SPL) is -34-（-192）=158 dB.

Table. S1. Sensitivity comparison of hydrogel-based mechanosensors.

Entry	Dielectric layer (wood-based)/ Transfer media	Electrode	Working mode	Sensitivity, kPa^{-1}	Ref.
1	Elastic ionic polyacrylamide hydrogel (EIPH)	Indium-tin oxide electrode	Microapacitive mechanosensors	2.33	[S1]
2	TA@ HAP NWs/$AlCl_3$ /PVA /ethylene glycol (EG)/water	NR	Ionic conductive strain sensors	GF = 2.84	[S2]
3	TOCNF/PVA/borax/$CaCl_2$	PVA hydrogel	Microapacitive mechanosensors	0.75	[S3]
4	A polyacrylamidehydrogel containing NaCl as the ionic conductor/acrylicelastomer (VHB)	Electrical double Layer	Ionic conductive sensors	1	[S4]
5	CNT forest elastic electrodes and intermediate elastic insulating layer	vCNT electrode	Microcapacitive mechanosensors	56.5	[S5]
6	A poly-(dimethylsiloxane) (PDMS) dielectric layer structure with tilted micropillar arrays	Au electrode	Microcapacitive mechanosensors	0.42	[S6]
7	Colorless polyimide (CPI)	Top AgNWs electrode and micropatterned bottom electrode	Microcapacitive mechanosensors	1.2	[S7]
8	C/ECH/NaCl	Copper foil	Microcapacitive mechanosensors	0.6	[S8]
This work	Amphibious dielectric hydrogel (Ni-CH) (conducting direct thermally-induced radical polymerization of PAAc in the presence of cellulose nanofibers (CNFs) on a thin nickel foam)	Carbon fiber electrode	Microcapacitive mechanosensors	182	This work

References

S1 M. J. Yin, Z. G. Yin, Y. X. Zhang, Q. D. Zheng and A. P. Zhang, Nano Energy, 2019, 58, 96-104.

S2 X. Jing, H. Li, H. Y. Mi, Y. J. Liu, P. Y. Feng, Y. M. Tan and L. S. Turng, SENSOR ACTUAT B-CHEM, 2019, 295, 159-167.

S3 X. Jing, H. Li, H.-Y. Mi, Y.-J. Liu, P.-Y. Feng, Y.-M. Tan and L.-S. Turng, SENSOR ACTUAT B-CHEM, 2019, 295, 159-167.

S4 J. Y. Sun, C. Keplinger, G. M. Whitesides and Z. Suo, Adv. Mater., 2014, 26, 7608-7614.

S5 U. H. Shin, D. W. Jeong, S. M. Park, S. H. Kim, H. W. Lee and J. M. Kim, CARBON, 2014, 80, 396-404.

S6 Y. Luo, J. Shao, S. Chen, X. Chen, H. Tian, X. Li, L. Wang, D. Wang and B. Lu, ACS Appl. Mater. Interfaces, 2019, 11, 17796-17803.

S7 Y. Wan, Z. Qiu, Y. Hong, Y. Wang, J. Zhang, Q. Liu, Z. Wu and C. F. Guo, Adv. Electron. Mater., 2018, 4, 1700586.

S8 X. Shen, D. Zhao, Y. Xie, Q. Wang, J. L. Shamshina, R. D. Rogers and Q. Sun, Adv. Funct. Mater., 2023, 33, 2214317.